Ocean Engineering 164 (2018) 55–64

Contents lists available at ScienceDirect

Ocean Engineering

journal homepage: www.elsevier.com/locate/oceaneng

The effects of oblique waves and currents on the loadings and performance of tidal turbines

Rodrigo Martinez*, Grégory S. Payne[1], Tom Bruce

School of Engineering, University of Edinburgh, UK

ARTICLE INFO

Keywords:
Tidal energy
Horizontal axis tidal rotor
Wave-current interaction
Performance characterisation
Tank testing
Physical modelling

ABSTRACT

Tidal energy exploitation is at an early deployment stage and costs need to be reduced to improve the long term economic viability of the sector. High costs of tidal turbines are, in part, the result of load uncertainties, which lead to the use of high factors of safety in the design to ensure survival. One of the most important causes of uncertainty is hydrodynamic loadings. To date, most of the scaled model experiments with horizontal axis turbines investigating this issue have been carried out with collinear wave and current directions. To the authors' knowledge, the work presented herein is the first experimental investigation of a horizontal axis turbine model subjected to combined oblique waves and current. Turbine performance and loading are measured for a 1:15 scale model tested in the FloWave circular, combined wave and current basin at the University of Edinburgh (UK). Three different flow directions were tested and each of them were also combined with regular waves in three different directions non-collinear with the flow. Fifteen physical quantities were measured including flow velocity, rotor and foundation loads and turbine speed. Characterisation of loads and turbine performance in those oblique current and wave conditions are presented. Waves affect means and standard deviation of rotor power and thrust, but off-axis waves are associated with lower thrust loads than head-on waves. Compared to current only, rotor torque and thrust standard deviations are higher in the presence of waves and almost twice as high when the wave crest is parallel to the rotor plan. The experimental data associated with this article can be downloaded from http://dx.doi.org/10.7488/ds/2360.

1. General introduction

Due to the ever greater urgency to address global warming issues, the Scottish Government (2013) has set a target of generating the equivalent of 100% of Scotland's electricity from renewable sources by 2020 with the added challenge of maintaining the country as a global lead in tidal and wave energy developments. Compared with other renewables such as wind and solar PV, tidal energy is at a relatively early stage on its maturity and needs continued research into fundamentals of machine loading and performance in realistic conditions to enhance reliability and cost effectiveness.

According to the Department of Energy and Climate Change (2013), the levelised cost of electricity (LCOE) from tidal stream sources is expected to reduce from 190£/MWh in 2025 to 171£/MWh by 2030 for shallow water deployments, and from 148£/MWh to 129£/MWh for deep water deployments. This is still not a competitive generation method compared to onshore wind turbines over 5 MW per unit which is forecasted to have in 2030 a LCOE of 97£/MWh. This is due to the high cost of capital expenditure (CapEx) and operational expenditure (OpEx). A solution to lower the LCOE is to reduce CapEx by optimising the structural design of the device whilst maintaining the device's performance and survivability. A possible approach is to lower the factors of safety (FS) that account for the design and performance uncertainties arising from loads in naturally occurring flows. A way to assess the effect of these loads is physical testing of scale models.

There is an extensive literature on tidal turbine testing based upon physical models. Bahaj et al. (2007) used a 0.8m rotor in a towing tank, finding that the highest performance for their tidal turbine model was at a tip-speed ratio (TSR) $\lambda = 5–7$ with pitch angle of 20°. They found that the power coefficient (C_P) of the turbine decreases as the rotor is yawed and when the turbine tip is around 0.19D from the water surface. Mycek et al. (2014), with a 0.7m rotor, Gaurier et al. (2013) with a 0.9m rotor and de Jesus Henriques et al. (2014) with a 0.5m rotor, all in a recirculating tank, observed that wave-induced fatigue loads show a standard deviation two to three times higher than for the current-only induced fatigue loads and represents a significant risk of failure. The average C_P and the average thrust coefficient (C_T) are however not affected. In addition, they found that the ambient turbulence affects the

* Corresponding author.
E-mail address: r.martinez@ed.ac.uk (R. Martinez).
[1] Present address: Department of Naval Architecture, Ocean & Marine Engineering, University of Strathclyde.

https://doi.org/10.1016/j.oceaneng.2018.05.057
Received 23 December 2017; Received in revised form 25 May 2018; Accepted 28 May 2018

fatigue loadings on the turbine, but not its performance. At higher turbulence intensity (TI), the wake was observed to recover faster than at lower TI. Luznik et al. (2013) with a 0.46m rotor tested in a towing tank, observed that in the absence of waves the turbine can operate at lower TSR values.

Evans (2014) and Easton (2013), using ADCP measurements at Ramsey Sound (Pembrokeshire, Wales, UK) and the Inner Sound (Pentland Firth, Scotland, UK) respectively, showed that the main flow direction at potential tidal sites can vary by up to 20° between flood and ebb. Their findings were used to inform the range of directionalities explored in the present work. In the field, although there is a predominant wave direction, there will be occasions when the wave direction varies from this. The wave direction is independent of the tidal flow direction. To the authors' knowledge however, the influence of waves not collinear to the current has not been explored in the literature, perhaps in part due to the limited number of testing facilities capable of producing such conditions.

The turbine model used for this project is described in Payne et al. (2017). The article details the design process of the turbine. Blade Element Momentum (BEM) is first used estimate the loads the turbine would be subjected to, which in turn informs the specifications for the force sensors and for the drive train. Finite Element Analysis (FEA) is used to ensure that the blades can structurally withstand the loads. Preliminary results from testing carried out in the recirculating flume of IFREMER in Boulogne-sur-Mer, France is also presented including C_P and C_T curves, load time series and wake measurements.

The tests for this project were carried out in the FloWave basin of the University of Edinburgh whose characteristics have been documented in Noble et al. (2015) and Sutherland et al. (2017). Both articles describe a fairly straight velocity depth profile from the surface up to mid-depth with slower speeds closer to the bottom of the basin. They observed that at 1.5m above the floor, the measured flow speed experiences significant spatial variation throughout the basin's raiseable floor area and it can be up to 50% lower than the prescribed value. The velocity depth profiles change considerably as the flow measurements are performed further away from the basin's centre, especially on the transverse direction to the flow. Significant changes become noticeable outside a ~5 meters radius. Noble et al. (2015) propose a working area of 8-by-6 meters outside of which the spatial variations are of the order of 10% of the nominal speeds. Inside this working area, all speed measurements are within 5% of the nominal speed.

The main objective of this study is to identify the effects of oblique waves and currents on the root bending moment of the blades, on the rotor thrust and torque loadings and on the performance of a tidal turbine. Presently, the use of Factors of Safety (FS) protect the devices from damage due to uncertain flow characteristics, the aim of this work is to reduce these design uncertainties. Tests were undertaken in a circular tank that allows the generation of waves and currents at any desired angle. This research used a 1.2 m diameter horizontal axis turbine model and a matrix of wave and current parameters ranging from collinear to oblique interactions. This work expands the findings from Martinez et al. (2017).

This work is divided in two main sections: flow characterisation and turbine testing. These sections are preceded by a general introduction of the testing facility and turbine model.

2. The experimental facility and turbine model

2.1. Wave-current basin and instrumentation

The FloWave facility, shown in Fig. 1, is located at The University of Edinburgh in Scotland, UK. It is a 25m diameter circular basin with a 2m working depth and a 15m diameter elevating floor to facilitate access to the basin bottom when setting up models. Current is generated by 28 5-bladed, 1.7m diameter impellers arranged around the full circumference of the basin. Multidirectional wave generation is archived by 168 absorbing flap type wavemakers, also arranged around the full circumference. This facility has the advantage of creating flow and waves independently at any given angle (Robinson et al., 2015). It was specifically designed to support tidal and wave energy research and development in intermediate water depths.

An Acoustic Doppler Velocimeter (ADV) was used for all flow measurements. The specific instruments used was a Vectrino Profiler from Nortek. This instrument can measure flow velocities up to 3.0 m/s at a sample rate of up to 100Hz.

Wave elevation are measured using resistive wave gauges. These are sampled at 64Hz and were calibrated every day before testing.

2.2. Turbine model

The turbine model used for the tests was designed and built by Payne et al. (2017) at the University of Edinburgh under The Engineering and Physical Sciences Research Council (EPSRC) funded project “X-MED” (EP/J010235/1). It consists of a 1:15 scale, 1.2m diameter rotor that represents an 18m diameter turbine at full scale. The blade profile is a NACA 63-8XX made of aluminium, manufactured by computer numerical control (CNC) machining. For these experiments, the turbine was operated under speed control. Fig. 2 shows the turbine mounted on the basin floor. All the instrumentation is kept protected inside the black and silver cylindrical sleeves.

The turbine was first tested at IFREMER in Boulogne-sur-Mer, France with results presented by Payne et al. (2017).

2.2.1. Turbine instrumentation

The turbine model is fitted with a transducer measuring rotor torque and thrust on the rotor only. It also includes sensors measuring the stream-wise root bending moment at the root of each blade. A resolver records the absolute angular position of the rotor. All the turbine sensors are sampled synchronously at 256Hz. The root bending moment load cells developed a fault during the tests and their measurements are therefore not analysed herein.

3. Flow characterisation

3.1. Introduction and methodology

In order to understand the onset flow the turbine was going to be exposed to, a campaign of flow characterisation tests was carried out before putting the turbine in the water. This section describes the tested conditions and findings.

Fig. 3 shows a top view of the basin, with a blue marker representing the location of the turbine. The dashed lines represent the wave angles selected and the solid, coloured lines, represent the flow angles. A flow speed of 0.8 m/s was selected. This is the design speed for the turbine model presented by Payne et al. (2017). From Froude scaling, this corresponds to a full-scale velocity of 3.1 m/s which, according to McNaughton et al. (2015), is a realistic flow speed for deployment sites such as the European Marine Energy Centre (EMEC). The wave directions were chosen to provide a broad range of conditions within the testing time allocated and the technical capability of the facility. In that context, tests in 180° opposing wave were not carried out as it limits the range of wave period available (because of the Doppler effect). 90° waves were also excluded because the associated wave induced velocity will be parallel to the rotor disc and will therefore have limited influence on its load. Wave heights and periods were chosen to produce (according to linear wave theory) a horizontal wave induced velocity at hub height of 0.1 m/s. Such a flow speed fluctuation is within the capability of the turbine model and would be associated at full scale with a 1.5m wave height and 8s wave period.

Wave heights and periods were selected to generate a wave-induced horizontal water particle velocity at hub height of 0.1 m/s. Three regular waves were used with the characteristics shown in Table 1.

Fig. 1. View of the FloWave basin.

Fig. 2. The turbine mounted on the basin floor (shown in the floor's raised position).

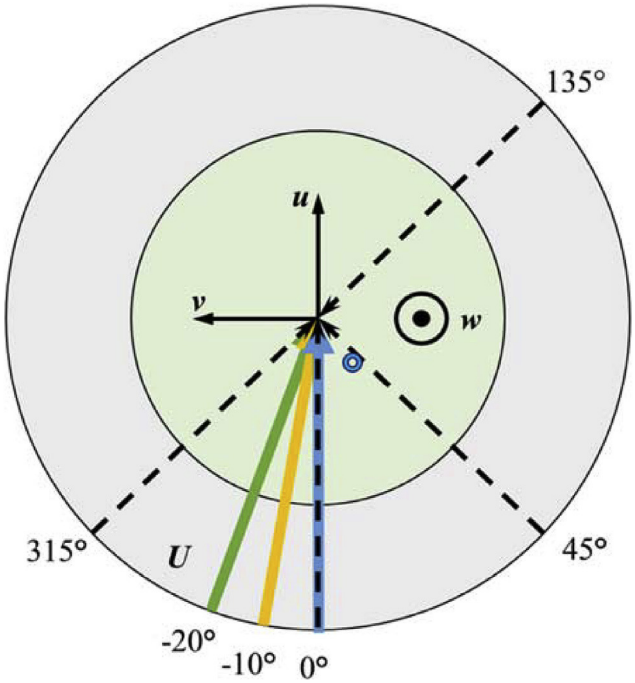

Fig. 3. Plan view of the basin indicating flow (solid) and wave (dashed) angles selected for testing. Blue marker represents the turbine position. (For interpretation of the references to colour in this figure legend, the reader is referred to the Web version of this article.)

These tests were performed without the turbine and measurements of the flow speed were taken in the plane where the rotor would be. Fig. 4 shows a front view of the rotor plane indicating where the wave gauges (yellow lines) were positioned during the tests and the flow velocity measurement positions (red markers) to create vertical and transverse profiles. The dashed circle represents the rotor swept area. The figure also shows the coordinate system used to describe the flow velocity components.

All the flow characterisation tests were recorded for 160s with a 32s ramp-up at the beginning to allow for the first waves generated to reach the centre of the basin, yielding an effective test duration of 128s after trimming off the run-up seconds.

Table 1
Wave parameters.

Period [s]	Wave height [mm]
2.0	102
2.5	91
3.0	86

3.2. Results

First, the case of no waves and zero yaw is considered. Fig. 5 shows

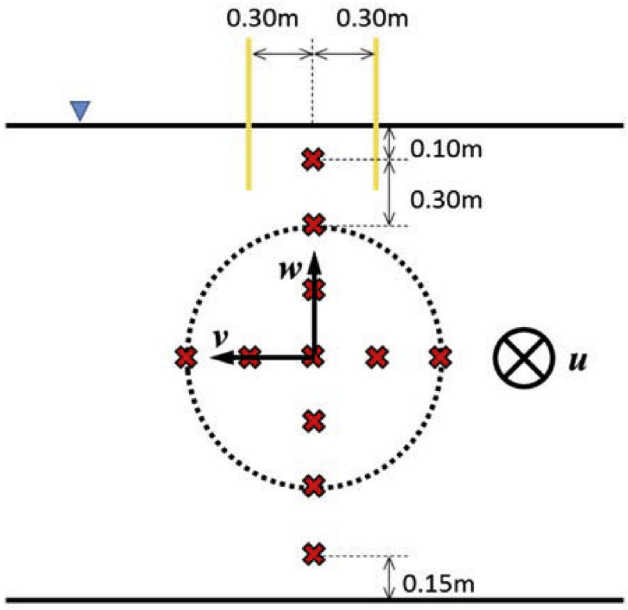

Fig. 4. Front view of the rotor plane delimited by the dashed circle. Wave gauges (yellow lines) and flow velocity measurement points (red crosses). (For interpretation of the references to colour in this figure legend, the reader is referred to the Web version of this article.)

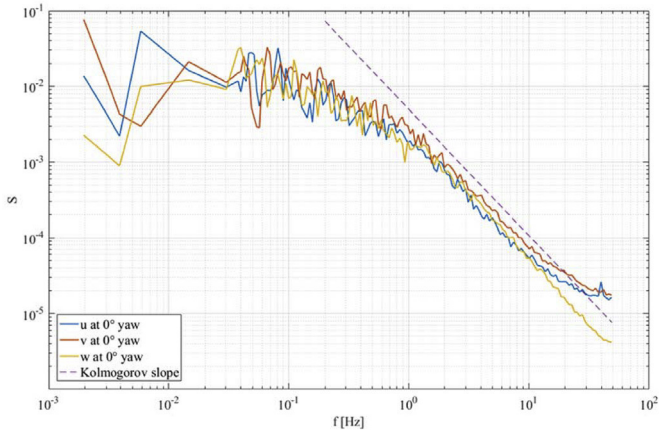

Fig. 5. Spectral comparison of the flow components at 0° without waves.

the spectral density of the onset velocity components $\boldsymbol{u}$, $\boldsymbol{v}$, and $\boldsymbol{w}$ at hub height plotted against frequency. Both axes use a logarithmic scale. These curves were obtained using a method where the data is down-sampled logarithmically, meaning that at lower frequencies, the bins contain fewer frequency components than at higher frequencies, giving smother curves at high frequencies. Two distinct regions of the spectrum are visible in the figure. For frequencies < 0.2 Hz, the trend of the spectra of the three velocity components is broadly horizontal, corresponding to the energy containing range. For higher frequencies, the fall away of the spectral density indicates the inertial range. All the velocity components are observed to follow closely the Kolmogorov slope of $-5/3$, indicating that measured flow is similar to the idealised case of 3D isotropic homogeneous turbulent flow conditions modelled by Kolmogorov's theory as presented by Thorpe (2007). The levelling-off of the spectra at the highest frequencies (above 30 Hz or so) is due to the limits of the instrumentation. This is discussed in Section 3.3.

The flow velocity magnitude $\boldsymbol{U}$ comprises both horizontal components of the flow ($\boldsymbol{u}$ and $\boldsymbol{v}$) and is defined by:

$$\boldsymbol{U} = \sqrt{\boldsymbol{u}^2 + \boldsymbol{v}^2} \tag{1}$$

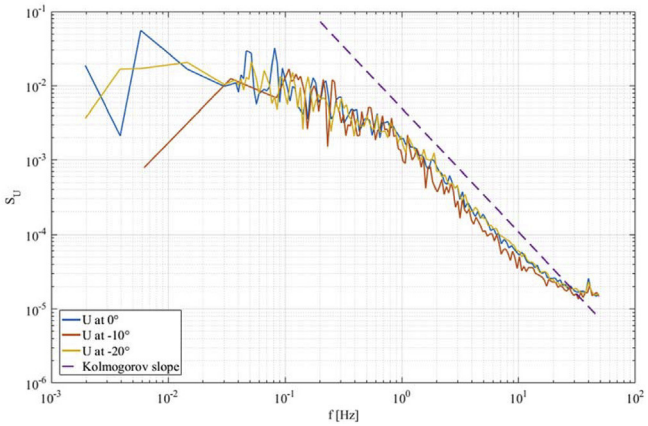

Fig. 6. Spectral comparison exploring the effect of yaw angle in **U** with no waves.

As the vertical flow component $\boldsymbol{w} < < \boldsymbol{u}, \boldsymbol{v}$ it was decided not to be included in $\boldsymbol{U}$.

Fig. 6 shows the spectral density of the onset flow velocity $\boldsymbol{U}$ at hub height without waves for three flow directions. The spectra are very similar for the three directions. Comparing Figs. 5 and 6, it can be seen that $\boldsymbol{U}$ has a similar spectral density to the individual velocity components, henceforth, $\boldsymbol{S_U}$ will replace the use of the components' spectra $\boldsymbol{S_u}$, $\boldsymbol{S_v}$ and $\boldsymbol{S_w}$.

Focussing on the $-20°$ yaw case, the influence of waves was explored by the addition of waves (period T = 2.0s; height H = 102 mm) from three different directions: 0°, 45° and 315°. Fig. 7 shows the resulting spectral density functions of the velocity $\boldsymbol{U}$. It is interesting to note the size of the spectral peaks associated with the wave period are about an order of magnitude higher than those associated with turbulence. This suggests that at the wave frequency, the energy contained in the waves is more significant than the energy contained in the turbulence.

In order to explore the uniformity of the flow within the rotor area and later on assess its effect on the turbine, the nine $\boldsymbol{U}$ point measurements located within the rotor area shown in Fig. 4, were calculated with **(1)**, time averaged and then spatial averaged, giving one single velocity value $\boldsymbol{U_0}$. Fig. 8 shows three different rotor area velocity maps. There are nine point measurements represented by red crosses. The dashed circle shows the rotor disc area. The subfigures are for flow at: *a)* 0°, *b)* $-10°$ and *c)* $-20°$ respectively. It can be seen that closer to the bottom of the basin the velocity is slower. This is due to bed friction-induced velocity shear profile and also due to the way in which the water is projected from the turning vanes in the basin - see Noble et al.

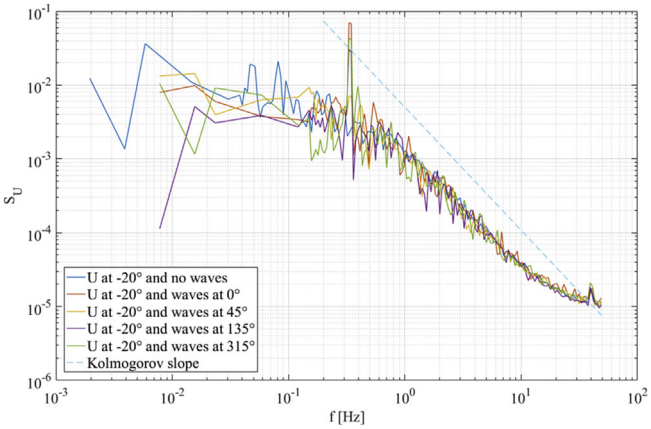

Fig. 7. Spectral comparison of **U** at $-20°$ with waves with T = 2.0s from all different directions.

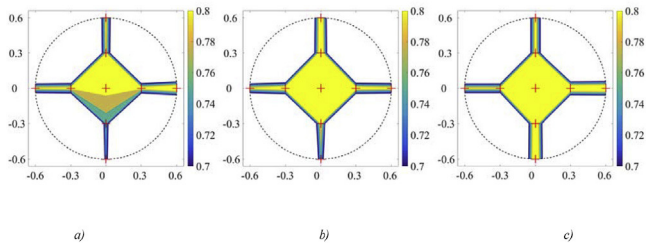

Fig. 8. Rotor velocities (**U**) maps for the 3 different flow angles. Colour bar units are m/s. a) 0° flow, no waves; b) −10° flow, no waves; c) −20° flow, no waves. (For interpretation of the references to colour in this figure legend, the reader is referred to the Web version of this article.)

(2015). It can also be observed that in the 0° and −20° cases, the right-hand side of the rotor disc experiences a faster flow with a relative increase to the rotor averaged velocity $\boldsymbol{U_0}$ of 8.5% and 7.7% respectively. The −10° case is more uniform throughout the rotor area although at the rotor axis, the velocity is slightly higher than the rotor area average. Bare basin measurements reported in Noble et al. (2015) and Sutherland et al. (2017) give the turbulence intensity varying between 5% and 11% in the stream-wise direction. All the cases show a transverse profile with the left-hand side showing slower velocities than the right side. On the other hand, 0° and −10° cases show also a depth profile that is not as pronounced in the −20° case. These variations in flow are not dissimilar to those of Noble et al. (2015).

3.3. Discussion

A feature of the spectral density data in Figs. 5–7 is an apparent levelling off for highest frequencies. The instrument's geometry shown in Fig. 9 is responsible for this artefact, the so-called “noise floor” seen in Fig. 6 where $\boldsymbol{u}$ and $\boldsymbol{v}$ curve start to become horizontal and detach from the −5/3 slope at around 10 Hz while the vertical component $\boldsymbol{w}$ keeps following the −5/3 slope up to 50 Hz. This is due to the 60° angle at which the probe's receivers are mounted relative to the emitter. The vertical direction is therefore “better aligned” with the receivers compared horizontal. This phenomenon was also observed by Harding et al. (2014). It is worth noting that the instrument was never rotated between tests and the basin velocity input values were always the same.

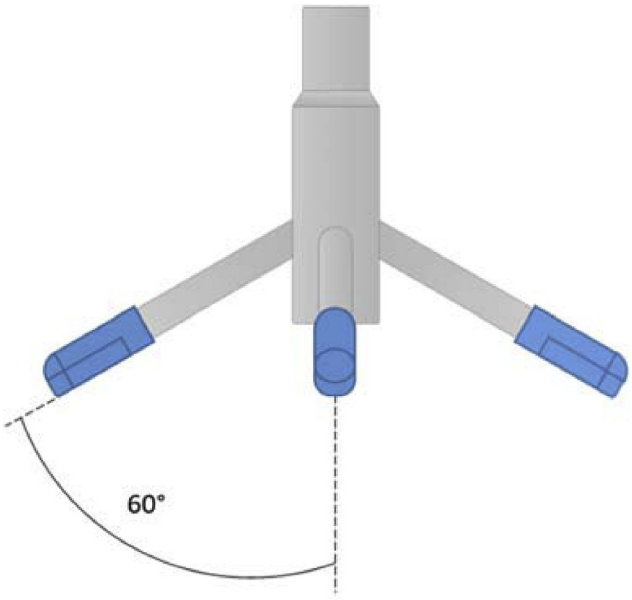

Fig. 9. Vectrino probe geometry. The emitter is located in the centre while four (only three shown in diagram) protruding arms represent the receivers.

Bare-basin testing gave a better understanding of how the flow behaves at the same position where the turbine sits. Although the flow showed some non-uniformity within the rotor area of the order of 10% or less, the quality of the data and the different conditions tested gave confidence that the data is fit for purpose and it was now possible to move on to the next stage of the data analysis with the turbine tests.

4. Turbine testing

4.1. Introduction

The objective of these tests is to determine how big an influence oblique waves and flows have on a horizontal axis turbine and to assist designers in choosing less conservative factors of safety. For this to happen it is necessary to understand how the conditions selected affect the performance and loadings of the turbine. The performance of the turbine is assessed through power and thrust coefficients across a range of tip speed ratio.

Turbine testing allows to understand the behaviour of the turbine loadings under oblique waves and currents, conditions that are poorly represented in the literature.

4.2. Methodology

The torque and thrust sensors were calibrated by the manufacturer. Previous experience has given confidence that the torque and thrust transducer show no drift during operation.

To improve the frequency analysis utilising fast Fourier transforms (FFT), the duration of each test was selected so that the number of measurement samples is a power of two. However, to allow for the waves to travel to the turbine's position, 30s had to be added to each test's duration but was removed prior to analysis.

From previous experience, operating the turbine below a particular TSR value in steady flow conditions leads to instability in the rotor's rotational speed as presented by Payne et al. (2017). Therefore, special care had to be taken while choosing the tests parameters. Here, a set of tests aimed at characterising turbine performance (C_P and C_T) across a range of TSR from 4.25 to 7.5 were performed. In these tests, the flow velocity remained fixed at 0.8 m/s and the rotor's speed was varied from 45 RPM and 95 RPM. It is thought that there is a hydrodynamic limitation that triggers instabilities for TSR < 4. All the turbine characterisation tests were performed without waves and at three different flow angles as shown in Fig. 10, and were based upon a measurement duration of 256s.

The location of the wave gauges (yellow markers) and Vectrino (red marker) relative to the turbine is shown in Fig. 11.

Shown in Fig. 3 are the flow and wave angles used for flow characterisation. These same conditions were also used for testing the turbine. The difference between the two sets of tests is that there is only one point measurement for the flow velocity, as shown in Fig. 12.

To limit the potential for damage to the turbine and its instrumentation, a cycle of tests was performed with the turbine configuration where all the load sensors were removed and replaced with dummy solid metal parts to make sure that the test program did not include conditions triggering the instabilities observed by Payne et al. (2017) in previous tests. Also, special care was taken during testing (with instrumentation) by constantly monitoring the live instruments' data stream looking for signal clipping or signals out of the expected range or shape.

All the loading tests were performed at a rated TSR of ~7 with prescribed flow speed of 0.8 m/s and 90 RPM, they were all recorded for 512s with a 33s buffer at the beginning to allow for the first waves generated to reach the centre of the basin.

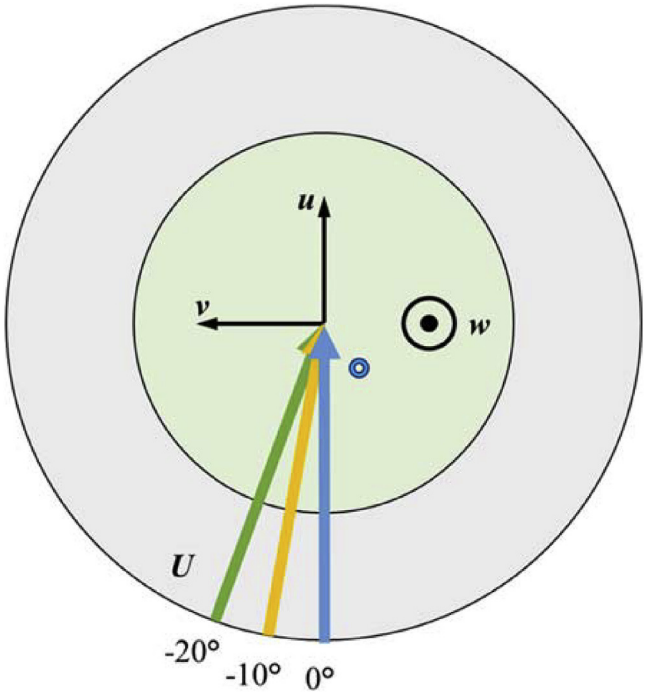

Fig. 10. Plan view of the basin indicating flow angles used during turbine characterisation and turbine position (blue marker). (For interpretation of the references to colour in this figure legend, the reader is referred to the Web version of this article.)

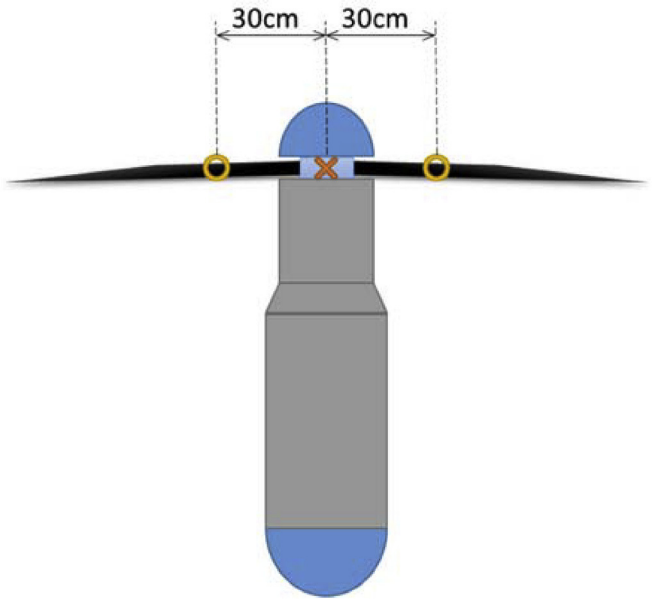

Fig. 11. Plan view of the turbine with position of instrumentation indicated by markers. Cross for ADV and circles for wave gauges.

4.3. Results

For calculating the power and thrust coefficients, C_P and C_T respectively, the following familiar definitions were used:

$$C_P = \frac{P}{\frac{1}{2}\cdot\rho\cdot A\cdot\overline{U_0^3}} \quad (2)$$

$$C_T = \frac{T}{\frac{1}{2}\cdot\rho\cdot A\cdot\overline{U_0^2}} \quad (3)$$

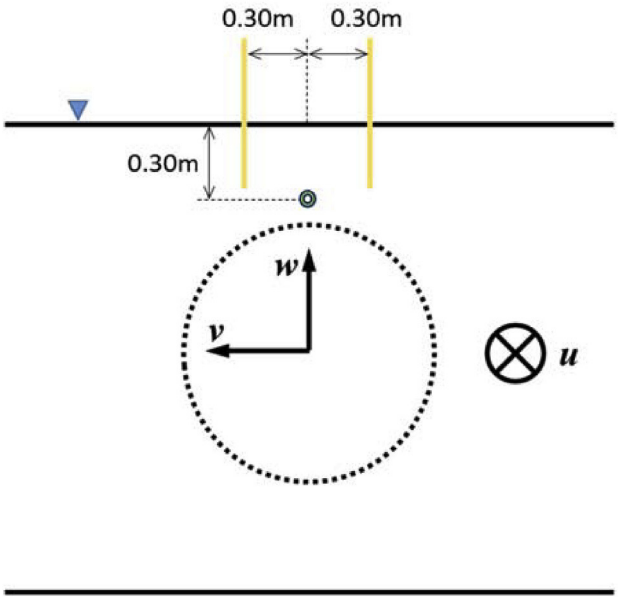

Fig. 12. Front view of the rotor plane shown by the dashed circle. Wave gauges (yellow lines) and flow velocity measurement point (green circle). (For interpretation of the references to colour in this figure legend, the reader is referred to the Web version of this article.)

where P is the power generated, T is the thrust experienced by the rotor ρ is the water density, A is the rotor area and, U_0 is the rotor-area-averaged flow velocity. Before calculating the spatial averaged $\overline{U_0^3}$ and $\overline{U_0^2}$, each single point measurement U needs to be calculated using equation **(1)**. For calculating $\overline{U_0^3}$ and $\overline{U_0^2}$, it is important to emphasise that each point measurement in the rotor area is cubed or squared before time averaging and then averaged over the nine measured points. This allows a more realistic representation of the flow as this method takes into account the dynamic nature of the flow and also gives a true RMS value as presented by Blackmore et al. (2016).

In Fig. 13 the C_T curves for flow at the three different yaw angles and without waves are presented against the TSR. Markers are the experimental data and the dashed lines show a quadratic fit. It is possible to note a decreasing trend that goes with the increasing yaw angle. The shadings in the background show the uncertainty bounds associated with standard deviation. The standard deviation is defined as the variation of the measurements from their mean and it is the square root of the variance.

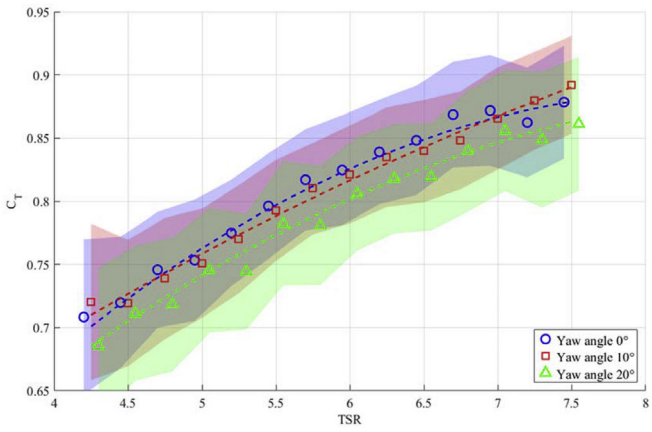

Fig. 13. Variation of C_T with TSR, for three yaw angles. No waves. The standard deviation associated with each yaw is shown using shading with the same colour as the data markers. (For interpretation of the references to colour in this figure legend, the reader is referred to the Web version of this article.)

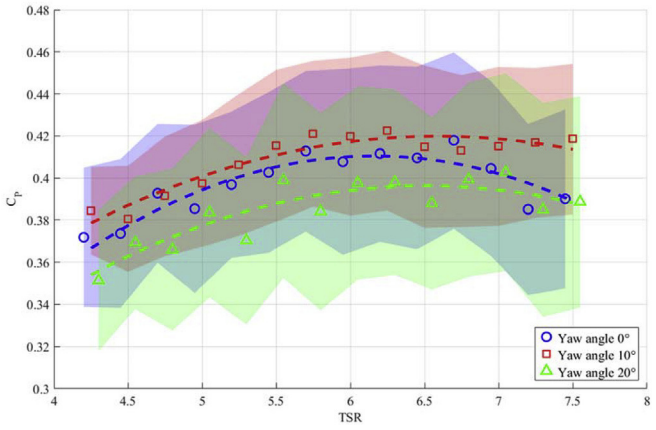

Fig. 14. Variation of C_P with TSR, for three yaw angles. No waves. The standard deviation associated with each curve is shown using shading with the same colour as the data markers. (For interpretation of the references to colour in this figure legend, the reader is referred to the Web version of this article.)

Fig. 14 shows the C_P variation with TSR for the same tests covering three yaw angles, without waves. Again, quadratic fits have been done to try to assist in the visual interpretation of the data. In this case, the curves do not follow the same intuitive variation with yaw that was followed by C_T. The red $-10°$ yaw angle curve has a higher C_P while the $-20°$ curve shows a considerably lower curve, with the 0° yaw curve lying between. This phenomenon was also observed by Frost (2016) but has not yet been satisfactorily explained. It could possibly be due to the significant variation in onset flow velocity observed over the rotor disc (see section 3.2). The flow characterisation used for the C_T and C_P calculations rely on only nine points. It is thought that using denser velocity mapping across the rotor area could yield different results.

It can be noticed that both C_P and C_T have very high standard deviation which arises from the high turbulence intensities and velocity variability across the rotor area.

Now introducing waves: Fig. 15 shows C_T and C_P for different flow yaw angle and for waves at 0°. The turbine TSR is 7 at nominal flow speed $\boldsymbol{U} = 0.8$ m/s. In this case the coefficients were calculated using rotor averaged $\boldsymbol{U_0}$ without waves. This approach helped identify the influence of the waves in the coefficients. It is possible to see the same trend in C_P as seen in Fig. 14 where the curve for the $-10°$ flow case is higher than 0° curve. For C_T, similarly to Fig. 14, both 0° and $-10°$ are very close to each other when waves are present. It is also worth noting how both 0° and $-10°$ decrease as the wave period increases but the $-20°$ flow case behaves the opposite way.

In Fig. 16, C_P and C_T curves for three flow angles with no waves and waves with T = 2.0 s at 0°, 45° and 315° are presented. For all, TSR = 7 and the flow speed is 0.8 m/s. As for Fig. 15, the coefficients were calculated using rotor averaged $\boldsymbol{U_0}$ without waves. Again, it is the cases at 0° and $-10°$ which show similar behaviour. The $-20°$ case follows the other two flow angles, contrary to Fig. 15. Here, comparing the same wave shows that as the waves' incidence angle increases, the coefficients decrease.

Plotted against frequency normalised by rotational frequency f_0, the C_T frequency spectra at TSR 7 and $\boldsymbol{U_0} = 0.8$ m/s (Fig. 17) where several noticeable peaks can be observed. The $-20°$ yawed flow was chosen to keep consistency with the other cases presented in this work, to see how big of an impact the most oblique flow has on the turbine. Following the spectra from left to right, the first large peak is associated with the wave frequency. The next peak at exactly $3f/f_0$ is the frequency with the passage of the three blades. Further harmonics of this at exactly 6, 9 and 12 f/f_0 are clearly identifiable, each with successively smaller amplitudes. The peak at 16 f/f_0 is believed to be caused by a mechanical artefact. Indeed, tests carried out at the same rotational speed but with the turbine outside the water ('dry test') show the same peak.

Fig. 18 shows a close up of the spectral peaks associated with the waves. The 45° and 315° peaks have similar amplitude which is consistent with them both being associated with wave conditions symmetrical with respect to the rotor axis. The peak at 0° shows the highest amplitude compared to the same wave at other angles. This is because the wave crest is parallel to the rotor plane. Therefore, the rotor experiences the whole force magnitude of the waves and not a component of this force.

Fig. 19 shows the C_P spectra at TSR 7 and $\boldsymbol{U_0} = 0.8$ m/s against the normalized frequency f/f_0. In this case the wave frequency and blade frequency ($3f/f_0$) peaks can be seen. The $6f/f_0$ peak is not believed to be a harmonic of the blade frequency since it is higher than the $3f/f_0$ peak. The $6f/f_0$ peak as well as the 18 f/f_0 and the 26 f/f_0 peaks are also present in 'dry tests' and are therefore not thought to be associated with fluid-blade interactions.

The mean and SD values for all the tests performed with waves with period T = 2.0s, TSR = 7 and $\boldsymbol{U_0} = 0.8$ m/s are presented in Table 2. At all flow angles, cases B, F and J with waves at 0° show the highest means and standard deviations for both torque and thrust compared to all the other cases with the same wave at different angles. The high SD values mean that the waves aligned with the rotor have a higher impact

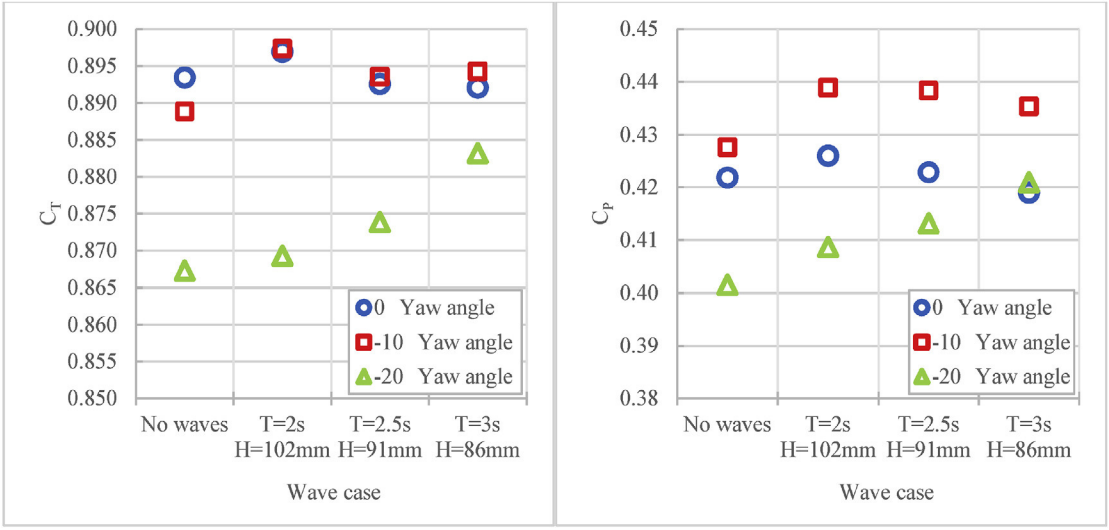

Fig. 15. C_T and C_P with all flow angles and all waves at 0° incidence.

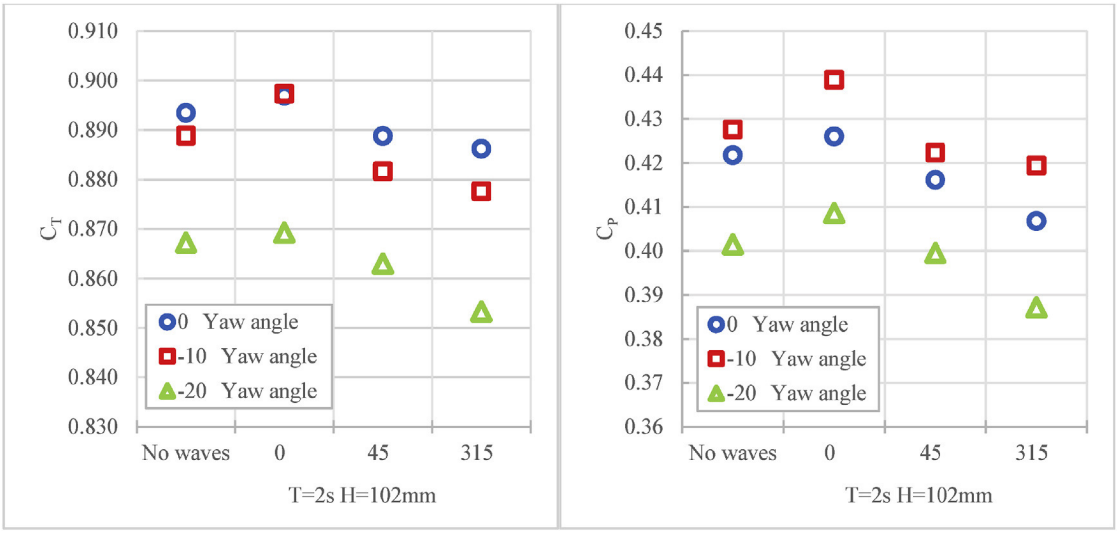

Fig. 16. C_T and C_P with flow at all angles and wave T = 2.0 s at all angles.

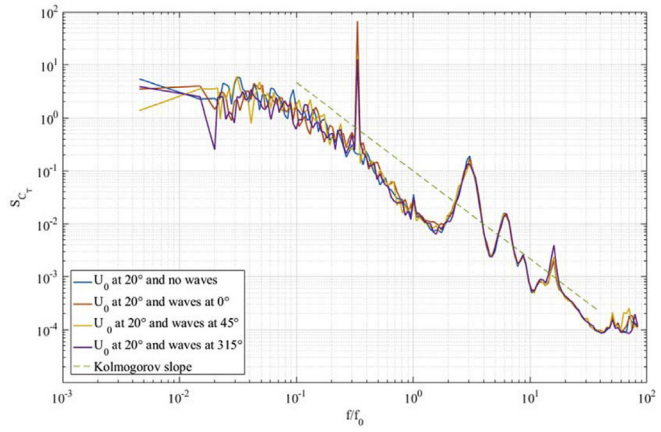

Fig. 17. C_T spectra with flow at −20°, exploring influence of wave angle.

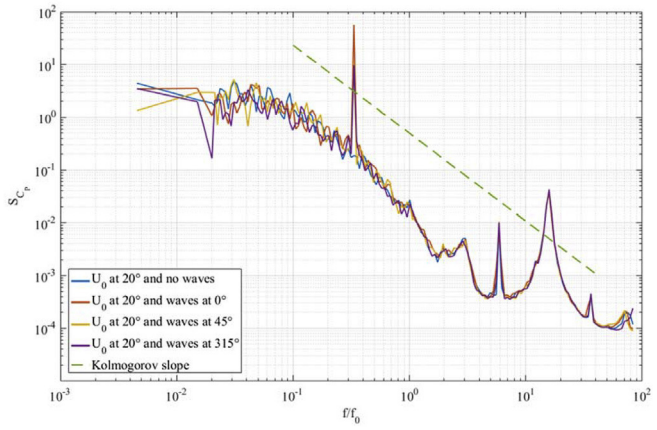

Fig. 19. C_P spectra with flow at −20°, exploring influence of wave angle.

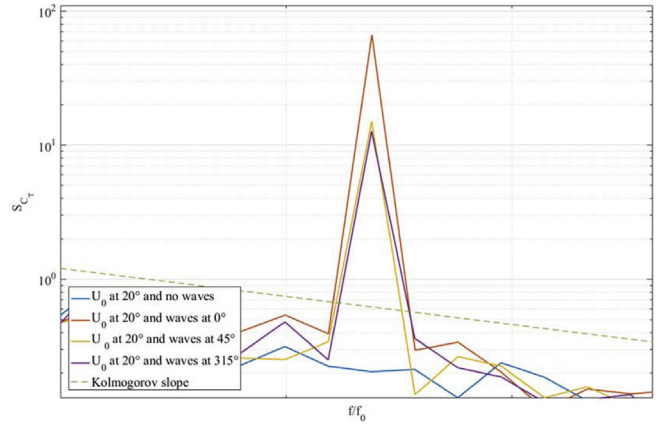

Fig. 18. Zoom of the peak of the C_T spectra associated with the waves with period T = 2.0s.

on the load variability because the rotor experiences the whole magnitude of the waves' forces and not a smaller component when the waves have an angle relative to the turbines axis. This will affect the fatigue loads directly. Cases D, H and L with waves at 315° show the lowest mean values for both torque and thrust. The difference between the values at 45° and the 315° cases is due to the relative angle between the flow and the wave. At 315° both have a NE direction while in the 45° case, the flow goes NE while the waves are moving NW. At all the flow angles, the cases with no waves have the lowest SD values for torque and thrust. The cases A, E and I with no waves show the lowest SD values.

Fig. 20 shows time series of wave elevation and rotor thrust for a test with nominal velocity $\boldsymbol{U}$ = 0.8 m/s, yaw angle −20°; waves T = 2.0s, H = 102 mm and wave angle 45°. It is possible to see how the low frequency component of the thrust signal follows the quasi period of the wave gauges, highlighting the influence of the wave on the thrust forces. The two wave gauges are slightly out of phase due to the angle of 45° at which the waves are generated. Looking at Fig. 11, it can be seen that when waves come at an angle other than perpendicular to the rotor plane, one of the wave gauges will 'sense' the wave sooner than the other wave gauge, giving a phase difference.

4.4. Discussion

The data presented in this section, proved to be of great use despite the faults with the root bending moment sensors and the high variability in the flow that accounted for such high SD on C_T and C_P. These values were expected after the non-uniformity presented on Section 3.

Turbine testing allowed to understand the impact of waves and current at different angles on the loadings and performance of the turbine. It is the standard deviation values of the torque and thrust that are highly affected by them. With flow at −20° and waves at 315° the torque has the lowest mean values. Flow at 0° with no waves has the

Table 2
Means and standard deviation of torque and thrust for all flow angles at **U** = 0.8 m/s and T = 2.0s waves at all angles. TSR = 7.

Line	Current		Waves			Torque [Nm]	SD Torque [Nm]	Thrust [N]	SD Thrust [N]
	U_0 [m/s]	Angle	Period T [s]	Height H [mm]	Angle				
A	0.78	0°	–	–	–	13.2	1.29	326	15.9
B	0.77	0°	2.0	102	0°	13.3	2.32	327	27.2
C	0.77	0°	2.0	102	45°	13.0	1.68	324	20.0
D	0.78	0°	2.0	102	315°	12.7	1.83	323	22.1
E	0.81	−10°	–	–	–	14.6	1.24	343	15.1
F	0.81	−10°	2.0	102	0°	15.0	2.52	347	28.8
G	0.80	−10°	2.0	102	45°	14.4	1.62	341	19.2
H	0.80	−10°	2.0	102	315°	14.3	1.91	339	22.1
I	0.77	−20°	–	–	–	13.2	1.60	327	18.9
J	0.77	−20°	2.0	102	0°	13.5	2.90	328	33.2
K	0.78	−20°	2.0	102	45°	13.2	1.90	326	22.5
L	0.77	−20°	2.0	102	315°	12.7	1.80	322	21.3

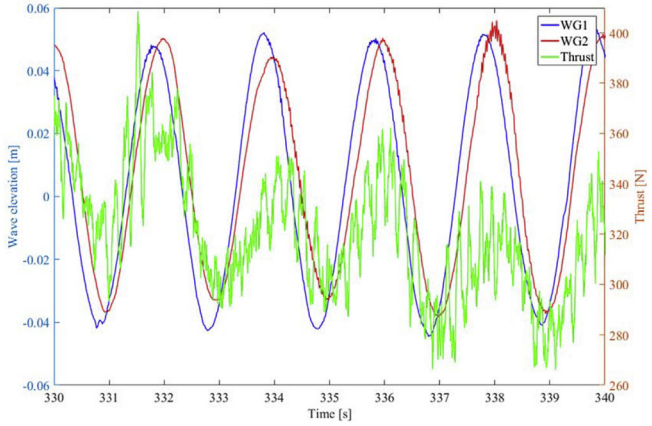

Fig. 20. Time series of both wave gauges (left y axis) and thrust (right y axis).

lowest SD values and any flow case with waves at 0° gave the highest means and SD. This tests reduce some of the uncertainties associated with the effect of the onset flow on a tidal stream turbine.

5. Conclusions

The work reported results from basin testing of a 1:15 scale horizontal axis tidal turbine in oblique currents and waves at FloWave. To the knowledge of the authors, the tests are the first of their kind.

The flow characterisation for the current only cases showed some flow velocity spatial variation across the rotor area. It was decided to use all the measurement points taken within the rotor area to give a better representation of the flow. The case with flow at −10° yaw had the highest C_P values, followed by 0° and −20°. Similar findings are reported by Frost (2016). This counterintuitive trend could be related to the significant velocity variations in the onset flow. The velocity value used in the computation of C_P and C_T are based on the nine measurement points across the rotor but a higher number of points within the rotor area would yield a more accurate representation of the onset flow which could have consequences on power coefficient values. These results show the importance of onset flow characterisation for turbine performance assessment.

The C_T at −10° showed the expected trend where the thrust coefficient decreases with flow angle.

The presence of waves, especially at 0° incidence to the turbine axis, leads to SD values for torque and thrust which are almost double those associated with current only. This would have a detrimental impact for fatigue loading. The mean values of the torque and thrust are however, hardly affect by waves compared to current only conditions.

Unlike the flow with yaw angles of 0° and −10°, −20° yawed current in combination with waves at 0° show an increase in the C_T and C_P with wave period. Once again, this trend should be treated with caution given the importance and uncertainties associated with the onset flow velocity used in the power and thrust coefficients calculations.

In the frequency analysis, the peaks in S_{C_T} and S_{C_P} associated with waves at 45° and 315° have similar magnitude which is consistent with the fact that these two wave directions are symmetrical with respect to the rotor axis. The peaks associated with the waves at 0° have the highest magnitude compared to all the other wave angles. The peaks associated with waves at 135° have the lowest magnitude.

The different parameters used to test the turbine covered a wide range of cases which could be found in the ocean and which, to the authors' knowledge, had not been tested at scale previously.

The findings presented herein provide original and important elements for considerations in the design process of tidal turbine. The spectral analysis of loads could be a key input for turbine components design and specifications. With a better understanding of the frequency distribution of loads, safety factors could be reduced and the turbine structure can be designed to ensure that no vibration mode corresponds to significant load frequencies.

Acknowledgments

The first author would like to acknowledge the financial support of Consejo Nacional de Ciencia y Tecnología (CONACYT). The authors would like to thank the FloWave staff, Jeff Steynor, Tom Davey and Martin Lennon, for their help with the testing. This work would not have been possible without the funding from the EPSRC via the Marine Challenge grant EP/J010235/1 (X-MED) for the development of the turbine model. The experimental data used to create the plots can be downloaded from http://dx.doi.org/10.7488/ds/2360.

References

Bahaj, A.S., Molland, A.F., Chaplin, J.R., Batten, W.M.J., 2007. Power and thrust measurements of marine current turbines under various hydrodynamic flow conditions in a cavitation tunnel and a towing tank. Renew. Energy 32 (3), 407–426. http://dx.doi.org/10.1016/j.renene.2006.01.012. Elsevier.

Blackmore, T., Myers, L.E., Bahaj, A.S., 2016. Effects of turbulence on tidal turbines: implications to performance, blade loads, and condition monitoring. Int. J. Mar. Energy 14, 1–26. http://dx.doi.org/10.1016/j.ijome.2016.04.017. Elsevier Ltd.

Department of Energy and Climate Change, 2013. Electricity Generation Costs. doi: 267393///1/1 25 May 2010.

Easton, M.C., 2013. An Assessment of Tidal Energy and the Environmental Response to Extraction at a Site in the Pentland Firth. University of Aberdeen.

Evans, P.S., 2014. Hydrodynamic Characteristics of Macrotidal Straits and Implications for Tidal Stream Turbine Deployment. PhD thesis. Cardiff University, Cardiff, UK.

Frost, C.H., 2016. Flow Direction Effects on Tidal Stream Turbines. PhD thesis. Cardiff University, Cardiff, UK.

Gaurier, B., Davies, P., Deuff, A., Germain, G., 2013. Flume tank characterization of marine current turbine blade behaviour under current and wave loading. Renew.

Energy 59, 1–12. http://dx.doi.org/10.1016/j.renene.2013.02.026. Elsevier.
Harding, S., Payne, G.S., Bryden, I., 2014. Generating controllable velocity fluctuations using twin oscillating hydrofoils : experimental validation. J. Fluid Mech. 750, 113–123. http://dx.doi.org/10.1017/jfm.2014.257. Cambridge University Press.
de Jesus Henriques, T.A., Tedds, S.C., Botsari, A., Najafian, G., Hedges, T.S., Sutcliffe, C.J., Owen, I., Poole, R.J., 2014. The effects of wave-current interaction on the performance of a model horizontal axis tidal turbine. International Journal of Marine Energy 8 (December 2014), 17–35. http://dx.doi.org/10.1016/j.ijome.2014.10.002. Elsevier Ltd.
Luznik, L., Flack, K.A., Lust, E.E., Taylor, K., 2013. The effect of surface waves on the performance characteristics of a model tidal turbine. Renew. Energy 58, 108–114. http://dx.doi.org/10.1016/j.renene.2013.02.022. Elsevier.
Martinez, R., Payne, G.S., Bruce, T., 2017. Preliminary results on the effects of oblique current and waves on the loadings and performance of tidal turbines. In: Proceedings of the 12th European Wave and Tidal Energy Conference. Cork, Ireland, pp. 1–8.
McNaughton, J., Harper, S., Sinclair, R., Sellar, B.G., 2015. Measuring and modelling the power curve of a commercial-scale tidal turbine. In: Proceedings of the 11th European Wave and Tidal Energy Conference, pp. 1–9.
Mycek, P., Gaurier, B., Germain, G., Pinon, G., Rivoalen, E., 2014. Experimental study of the turbulence intensity effects on marine current turbines behaviour. Part I: one single turbine. Renew. Energy 66, 729–746. http://dx.doi.org/10.1016/j.renene.2013.12.036. Elsevier Ltd.
Noble, D.R., Davey, T.A.D., Smith, H.C.M., Kaklis, P., Robinson, A., Bruce, T., 2015. Spatial variation in currents generated in the FloWave ocean energy research facility. In: Proceedings of the 11th European Wave and Tidal Energy Conference, pp. 1–8.
Payne, G.S., Stallard, T.J., Martinez, R., 2017. Design and manufacture of a bed supported tidal turbine model for blade and shaft load measurement in turbulent flow and waves. Renew. Energy 107, 312–326. http://dx.doi.org/10.1016/j.renene.2017.01.068. Elsevier.
Robinson, A., Ingram, D.M., Bryden, I., Bruce, T., 2015. The generation of 3D flows in a combined current and wave tank. Ocean Eng. 93, 1–10. http://dx.doi.org/10.1016/j.oceaneng.2014.10.008. Elsevier.
Sutherland, D.R.J., Noble, D.R., Steynor, J., Davey, T.A.D., Bruce, T., 2017. Characterisation of current and turbulence in the FloWave ocean energy research facility. Ocean Eng. 139 (2), 103–115. http://dx.doi.org/10.1016/j.oceaneng.2017.02.028. Elsevier.
The Scottish Government, 2013. 2020 Routemap for Renewable Energy in Scotland - Update. Edinburgh. Available at: http://www.gov.scot/Resource/0044/00441628.pdf.
Thorpe, S.A., 2007. An Introduction to Ocean Turbulence, an Introduction to Ocean Turbulence. Cambridge University Press, Cambridge. http://dx.doi.org/10.1017/CBO9780511801198.